J Mater Sci (2016) 51:7966–7976

Ultra-low-κ HFPDB-based periodic mesoporous organosilica film with high mechanical strength for interlayer dielectric

Jiawei Zhang[1,2], Guoping Zhang[1,*], Yongju Gao[1,2], Rong Sun[1,*], and C. P. Wong[3,4]

[1] Shenzhen Institutes of Advanced Technology, Chinese Academy of Sciences, Shenzhen, China
[2] Nano Science and Technology Institute, University of Science and Technology of China, Suzhou, China
[3] School of Materials Science and Engineering, Georgia Institute of Technology, 771 Ferst Drive, Atlanta, GA 30332, USA
[4] Faculty of Engineering, The Chinese University of Hong Kong, Shatin 999077, Hong Kong, China

Received: 3 February 2016
Accepted: 12 May 2016
Published online: 24 May 2016

ABSTRACT

A novel bridged organosilane precursor with star-shaped construction, [hexfluoropropane-2,2-diyl)dibenzyl-bridged organosilane (HFPDBO)], is prepared by facile organic synthesis method. The resultant HFPDBO precursor is mixed with porogen and acid catalyst to prepare periodic mesoporous organosilica (PMO) thin film via evaporation-induced self-assembly after spin-coating procedure. All the as-prepared HFPDB-based PMO thin film has been characterized by Fourier transform infrared spectroscopy, nuclear magnetic resonance spectrum, scanning electron microscopy, transmission electron microscope, and small-angle X-ray diffraction, respectively. Thereinto, the HFPDB-based PMO thin film with weight ratio of porogen to precursor (0.75:1) possesses excellent dielectric property (1.58@1 MHz of dielectric constants), high mechanical property (5.54 ± 0.11 GPa of Young's modulus) and hydrophobic property (90.1° of water contact angle) simultaneously. These low dielectric constant, high mechanical strength, and the hydrophobicity suggest potential application of the HFPDB-based PMO thin films as low-k materials in microelectronics.

Introduction

To reduce the resistive-capacitive time delay (RC delay) caused by parasitic resistance and parasitic capacitance, replacing Al metal wire with Cu and introducing lower dielectric constant (k value) materials as interlayer dielectric (ILD) into an integrated circuit (IC) have stry. Up to now, reducing the dielectric constant of the ILD can be considered as one promising solution. Some scientists devoted their attempts to developing novel ILD with ultra-low dielectric constant [1–3]. As well as known, the existing low-κ materials can be simply divided into

Address correspondence to E-mail: gp.zhang@siat.ac.cn; rong.sun@siat.ac.cn

DOI 10.1007/s10853-016-0066-6

"Non-Si" and "Si-based" [4]. The "Si-based" low-κ materials as ILD have attracted much attention because of their dielectric and compatibility with processes of IC manufacturing. Furthermore, the κ value of "Si-based" low-κ materials varies from about 2.0 to 4.0 according to the composites and microstructure [5], for example silicon dioxide (SiO_2 4.0), silicon oxycarbides (SiCOH 2.7–3.0)[6, 7], hydrogen-SSQ (HSSQ 3.0–3.2), methyl-SSQ (MSSQ 2.7–2.9) [8, 9], polyhedral oligomeric silsesquioxane (POSS 2.0–2.20) [10]. However, according to the report established by ITRS in 2009, it is needed to develop ultra-low-κ materials with a state-of-the-art value ultimately lower than 2.0 to meet the demand of multifunctional IC [11].

It is well known that these are two feasible ways for reducing κ-value, decreasing polarity and density. First, reducing polarity is for decreasing dipole strength and number of dipoles, so some less polar bonds, like C–C and C–F, are used to instead higher polar group [2]. Compared with low polarity, low density, meaning high porosity, is much more beneficial to decreasing dielectric constant. The porosity drastically reduces the κ value because the pores are filled with air, which has the lowest κ value of almost 1 [12]. However, higher porosity deteriorates the mechanical properties of material, which cannot meet the basic requirements of following process of chemical mechanical polish (CMP) [13]. Therefore, developing promising ultra-low-κ material with excellent mechanical strength simultaneously is desirable [14–16].

Compared with conventional silica-based ILD, periodic mesoporous organosilica (PMO) has immeasurable potential in terms of dielectric constant and mechanical properties [17–19]. PMO possesses ordered mesoporous structure with pore diameter between 2 and 50 nm according to IUPAC definition [20] and organic groups are uniformly distributed into the pore wall. Therefore, PMO with unique structure and functional groups was comprehensively investigated as ultra-low-κ material, which can be considered as promising solution for next generation IC [2, 21, 22]. Precursor 1,2-bis(triethoxysilyl)ethane (BTEE) with C–C bridged unit was coated for preparing PMO thin film, and poly(ethylene oxide)-poly(propylene oxide)-poly(ethylene oxide) (P123) was used as porogen to improve porosity and decrease dielectric constant ($\kappa = 1.8$) also with high Young's modulus ($E = 6.27$ GPa) [23]. Similarly, precursor polybenzoxazine-bridged polysisesquioxanes (PBz-BPSSQ) was developed to prepare PMO film previously, which exhibits remarkable dielectric property ($\kappa = 1.57$@1 MHz) but not good mechanical strength ($E = 3.1$ GPa) [24]. Furthermore, A. Ozin's group developed POSS-based precursor to prepare PMO thin film via evaporation-induced self-assembly (EISA) method [14]. Introducing POSS with nano-sized (0.3 nm) cage structure pore into the pore walls of PMO film was helpful to increase the porosity and reduce the κ value ($\kappa = 1.73$@1 MHz) with ordinary mechanical property ($E = 3.30$ GPa), which is slightly smaller than the stiffness limit of 4 GPa required for CMP [14, 16]. Although the dielectric properties of PMO materials were improved significantly, the mechanical properties still cannot meet the demands of practical application for IC manufacturing [25–28].

In this work, we have developed a novel bridged organosilane precursor (hexfluoropropane-2,2-diyl)dibenzyl-bridged organosilane (HFPDBO) by a facile organic synthesis method successfully. The resultant HFPDBO precursor with star-shaped construction and tetrafunctional organosilane branches was mixed with ethanol, acid and porogen to prepare coating solution for spin-coating, which was via an EISA method to prepare HFPDB-based PMO thin film. Furthermore, the microstructure, crystallization, dielectric, thermal, mechanical, and hydrophilic properties of all HFPDB-based PMO films were investigated comprehensively.

Experimental

Materials

2,2-Bis(3-amino-4-hydroxyphenyl)hexafluoropropane (BAHP, 95 %) was obtained from TCI Shanghai Development Co Ltd., China. 3-(Triethoxysilyl)propyl isocyanate (TPI, 95 %) was supplied by Aladdin industrial Co Ltd., China. Polyoxyethylene (4) lauryl ether (Brij® L4, M_w 362) was purchased from Sigma-Aldrich Co. LLC., China. Acetone and ethanol were obtained from Sinopharm Co Ltd. and purified with molecular sieve before use. N-type (111) silicon wafer (0.001–0.004 Ω) was obtained from Suzhou resemi Co Ltd. All other reagents and materials were used as received.

Synthesis of the (hexfluoropropane-2,2-diyl) dibenzene-bridged organosilane (HFPDBO)

In order to complete reaction, 0.92 g (2.5 mmol) of BAHP powder was added into 10 mL of acetone and dissolved as solution. TPI solution was prepared by mixing 2.72 g (11.0 mmol) of TPI with 5 mL of acetone. Then, the BAHP solution was added dropwise into the TPI solution slowly under condition of dry nitrogen. The reaction temperature can be controlled by drop speed and the reaction was kept in ice bath for 2 h after drop ending. At last, mechanically stirring should be continued for another 4 h at room temperature. Finally, the HFPDBO precursor was purified by column chromatography with 87.9 % of productive yield.

Preparation of the periodic mesoporous HFPDB-based PMO thin films

The HFPDBO precursor solutions for preparing PMO thin films were prepared as shown in Table 1. First, the purified HFPDBO (0.68 g, 0.5 mmol) precursor was added into 2 mL of acetone to prepare precursor solution. Then the Brij® L4 was added into ethanol to prepare porogen solution with concentration of 0.34 g/mL, and different volumes of porogen solutions were mixed with precursor solution to vary the weight ratios of porogen to precursor from 25, 50, 75 to 100 %, respectively. Then, moderate ethanol was added into resultant solution for adjusting the concentration of HFPDBO in each sample to maintain consistently; then 0.5 mL of HCl (1 M) was added into every solution under stirring for 30 min in order to obtain uniform precursor solution. Before spin-coating, substrates should be rinsed by cleaning agent propylene glycol monomethyl ether (PGME) and blow-dried with pure nitrogen. The as-prepared precursor solution was spin coated at rotary speed of 900 r.p.m. for 30 s. The resulting film was dried in air at room temperature overnight and then was heated at 60 °C for another 48 h under flowing nitrogen to increase the degree of condensation of the hydrolyzed HFPDBO precursor. Next, the Brij® L4 template was extracted by washing the film with a solution of ethanol at 60 °C for 1 h. After the extraction, all samples were calcined at 300 °C for 6 h under flowing argon to remove residual porogen and yield HFPDB-based PMO thin film. For convenience, the as-prepared HFPDB-based PMO thin films with different weight ratios of porogen to precursor from 25, 50, 75 to 100 %, which can be named as H25, H50, H75, and H100, respectively.

Characterization

Nuclear magnetic resonance (NMR) spectrum was confirmed by AVANCE III 400 NMR spectrometer. Mass spectrogram was confirmed by SHIMADZU LC-20A high-performance liquid chromatograph (HPLC). Fourier transform infrared (FT-IR) spectrum (KBr) was measured using a Bruker Optics VERTEX 70 Fourier transform infrared spectrometer. The transmission electron microscope (TEM) images were confirmed by FEI Tecnai G2 F20 S-Twin TEM; samples were scraped from substrates and dispersed in ethanol and then were drop-casted on lacey copper grid; ethanol was required to evaporate thoroughly before imaging. The scanning electron microscope (SEM) images were taken on FEI Nova NanoSEM 450 field emission SEM; the sample was sputtered with a 10 Å thick gold coating before loading into the SEM chamber. Small-angle X-ray diffraction (XRD) patterns were recorded on Rigaku D/MAX-2500/PC X-ray powder diffractometer with Cu Kα radiation ($\lambda = 0.15406$ nm). The dielectric properties were measured by Agilent 4294A RF impedance analyzer and Keithley 4200-SCS four-point probe measurement. The mechanical properties characterization was performed on Hysitron TI Premier nano-indentation with applied force from 100 to 200 μN, and we tested random eight points each sample to promise the accuracy. The thermal properties were performed on Mettler-Toledo thermo gravimetric analyzer-differential scanning calorimeter (TGA-DSC), which

Table 1 Fabrication of HFPDBO precursor solutions

Sample	HFPDBO precursor	Brij® L4 solution (0.34 g/mL)	Ethanol	HCl (1 M)
H25	0.68 g	0.5 mL	1.5 mL	0.5 mL
H50	0.68 g	1.0 mL	1.0 mL	0.5 mL
H75	0.68 g	1.5 mL	0.5 mL	0.5 mL
H100	0.68 g	2.0 mL	0.0 mL	0.5 mL

was run from 30 to 900 °C at heating rate of 10 °C/min. Besides, contact angle was pictured using Dataphysics OCA20 optical contact angle measuring device.

Results and discussion

Due to highly reactive activity between –NCO and –OH (or –NH), the active hydrogen of BAHP can be substituted completely by TPI to form four-substituted organosilane precursor through controlling the stoichiometric ratio of reactants under mild condition as shown in Fig. 1a. Based on the specially molecular design of HFPDBO, C–F bond from hexafluoropropane group between benzene ring not only helps reduce polarity but also larger steric hindrance of hexafluoropropane confines the rotation of molecular chain as shown in Fig. 1b. Therefore, the rigid structure of HFPDBO precursor is beneficial to promoting periodic structure as well as mechanical strength [29, 30]. Because increasing the degree of polycondensation would better the mechanical properties [30], compared with traditional bifunctional precursors, tetrafunctional alkoxysilane groups of HFPDBO are able to improve the degree of polycondensation and the density of Si–O–Si unit, which promise good mechanical properties. Therefore, the novel HFPDBO precursor can be considered as promising candidate for preparing PMO film with excellently integrated properties.

The successful synthesis of HFPDBO precursor was confirmed by NMR spectra with sample dissolved in deuterated dimethyl sulphoxide (DMSO) as shown in Fig. 2. First, the [1] H-NMR spectrum had a strong resonance peak at $\delta = 1.22$ ppm corresponding to the methyl hydrogen atoms and another strong peak at $\delta = 3.80$ ppm corresponding to the methylene hydrogen atoms of alkoxy. Besides, peaks at $\delta = 8.16$, 8.34, and 8.66 ppm corresponding to the hydrogen atoms of imino group is present simultaneously which also can be considered as the most powerful evidence for the successful synthesis of precursor (Fig. 2a). Furthermore, [13] C-NMR spectrum with specific peaks at $\delta = 7.68$, 15.76, 18.84, 42.45, 58.17, 63.41, 103.50, 123.12, 128.87, 133.16, 139.92, 146.18, 155.14, and 158.48 ppm testified the complete signal of carbon atoms of HFPDBO (Fig. 2b). The molecule of precursor can also be testified by Mass spectrogram (Figure S1). Meanwhile, FT-IR was used to further confirm the successful synthesis of HFPDBO precursor as shown in Fig. 3a. It can be seen that characteristic peaks at 3416 and 3344 cm^{-1} ascribed to $–NH_2$ and –OH groups from BAHP and characteristic peaks at 2270 cm^{-1} corresponded to –NCO group from TPI disappeared in the spectrum of HFDPBO. Furthermore, characteristic peaks at 1616 and 1653 cm^{-1} can be ascribed to the

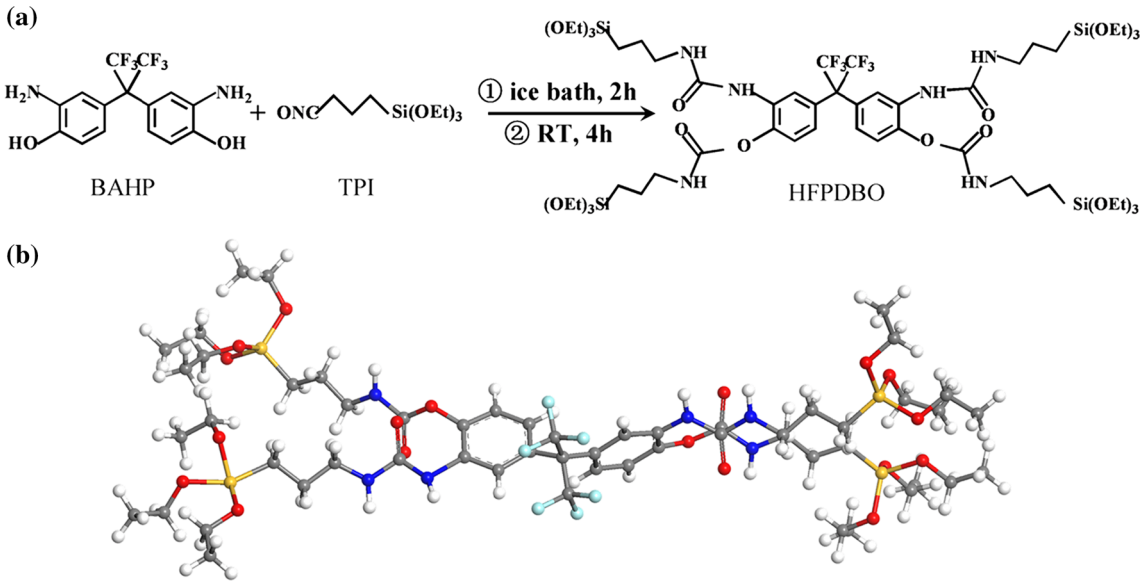

Figure 1 **a** Synthetic procedure of HFPDBO precursor and **b** 3D structure of HFPDBO precursor.

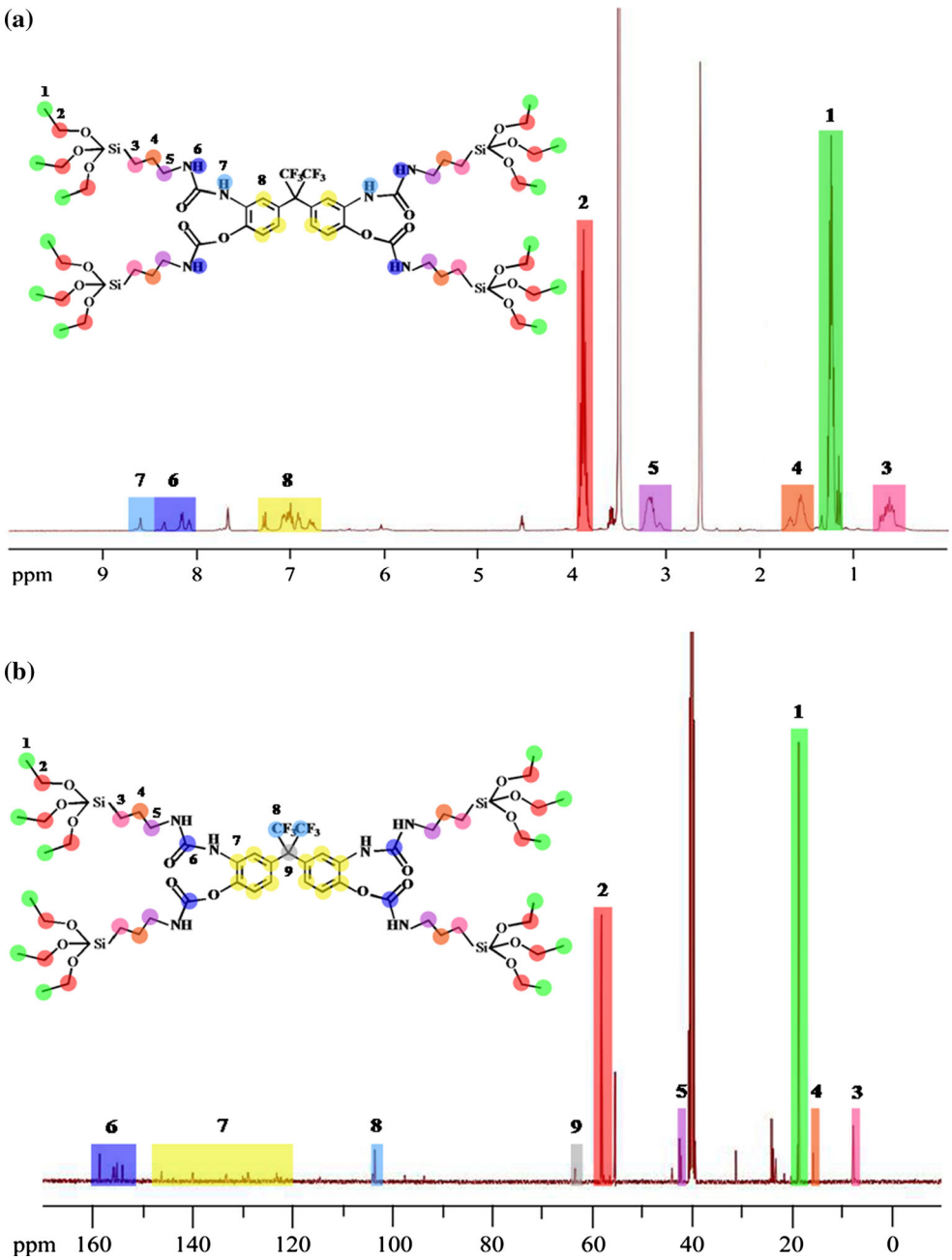

Figure 2 **a** ^{1}H-NMR and **b** ^{13}C-NMR spectra of HFPDBO precursor.

vibration of C=C group of benzene ring from BAHP, and the absorption peaks around 1700 cm^{-1} corresponding to C=O group which combine with near one, so the peak at 1653 cm^{-1} of HFPDBO precursor appears broader. Moreover, peaks at 1134 and 1034 cm^{-1} of precursor are clear, corresponding to –Si–O group [12, 24]. All of these features confirmed that the HFPDBO precursor had already synthesized successfully.

After successful synthesis of precursor, a schematic preparation procedure of HFPDB-based PMO thin film is depicted in Scheme 1. The precursor solution was mixed with porogen, Brij® L4, hydrochloric acid aqueous solution, and ethanol at a predetermined, optimized ratio under stirring for 30 min at room temperature. Brij® L4, a kind of nonionic surfactant, is liquid at room temperature with flash point at 113 °C. Therefore, Brij® L4 dissolved facilely in precursor solution and is accessible to be removed in the process of extraction and calcination, which are beneficial to form periodic pore for the EISA method. The HFPDB-based PMO thin film was prepared after

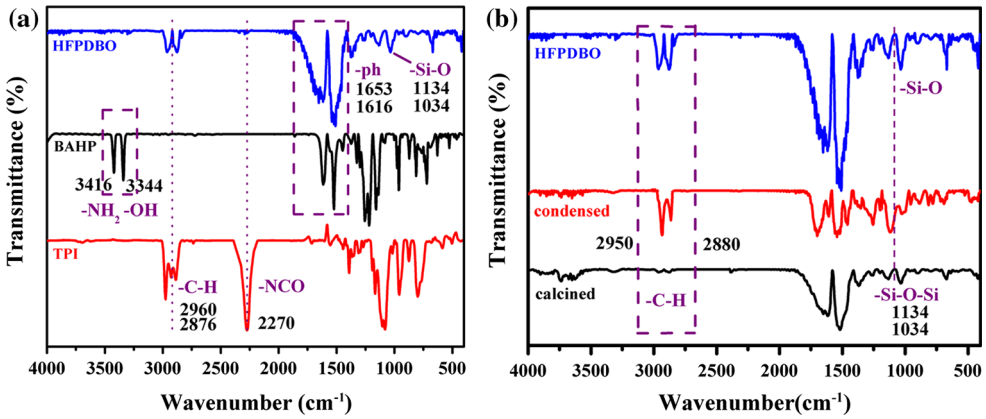

Figure 3 FT-IR spectra **a** of raw materials as well as HFPDBO and FT-IR spectra **b** of as-condensed as well as calcined HFPDB-based PMO film.

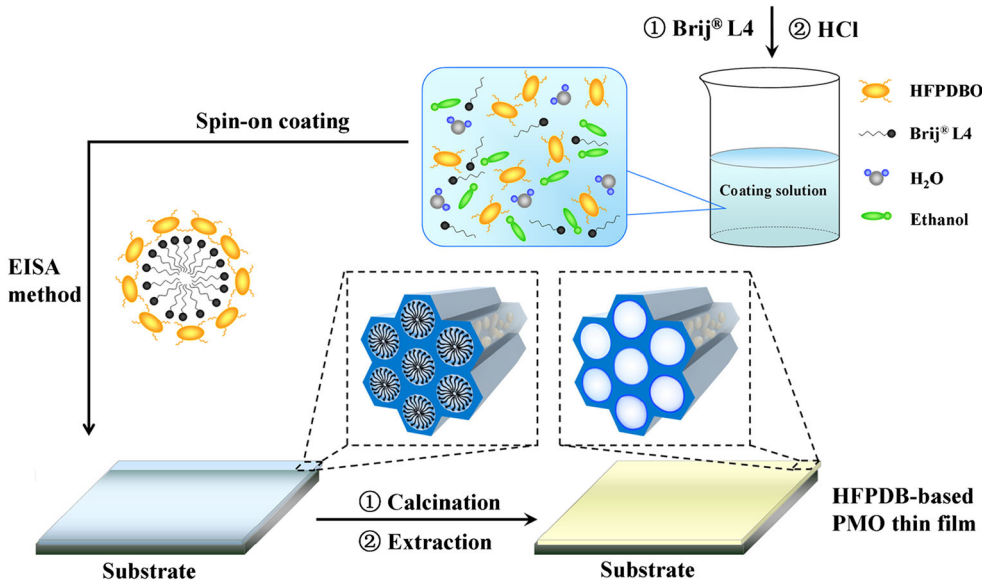

Scheme 1 Schematic illustration for the preparation of HFPDB-based PMO thin film using an EISA spin-coating procedure.

condensation, extraction and calcination processes. With the remove of porogen in the process of forming periodic pore structure, the condensation reaction between –Si–$(OEt)_3$ groups was underway until from the pore wall with –Si–O–Si– and bridged organic groups. Compared the FT-IR spectra of HFPDBO and PMO film at different stages, the characteristic peaks at 2880 and 2950 cm^{-1} corresponding to –C–H bond of alkoxy disappeared nearly in the spectrum of calcined PMO film as shown in Fig. 3b.

The morphology and cross section of as-prepared HFPDB-based PMO thin films were characterized by SEM as shown in Fig. 4. It can be seen that the HFPDB-based PMO thin films are smooth. With the content of porogen Brij® L4 increasing up to 75 %, little change emerges in the surface of samples H25, H50, and H75 (Fig. 4a–c). However, monodispersed PMO particles with diameter of around 60 nm appeared when the content of porogen was increased up to 100 % as shown in Fig. 4d, which can be ascribed to that the content of porogen is beyond the critical micelle concentration of precursor solution and leads to aggregated PMO particle with certain crystalline property [31, 32]. At last, all the inset pictures mean that there is not any obvious defect in the structure of PMO film with thickness between 500 and 600 nm mostly.

Figure 5a shows the typical small-angle XRD patterns of as-synthesized HFPDB-based PMO thin film with different weight ratios of porogen to precursor from 25 to 100 %, respectively. It is interesting to note that the sharp peak appears at 2θ around 1.3°, which is of characteristic of an ordered hexagonal material. The diffraction peaks of film samples are consistent

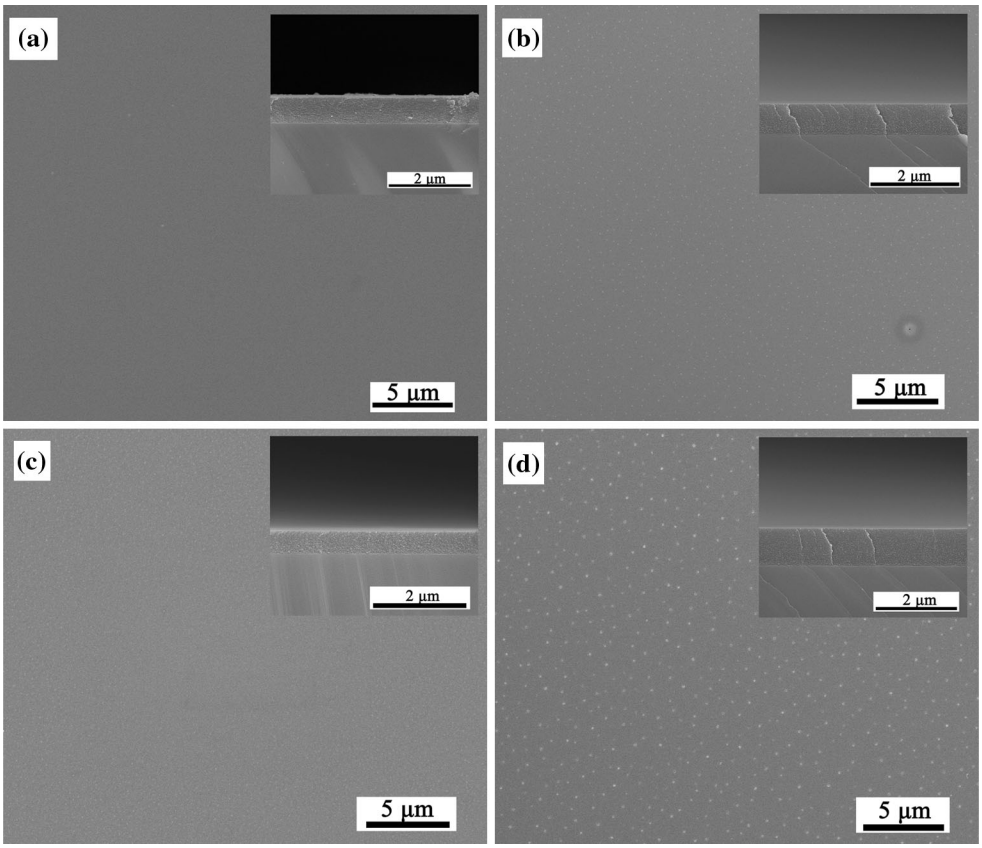

Figure 4 SEM images of surface of different HFPDB-based PMO thin films, **a** H25, **b** H50, **c** H75, **d** H100.

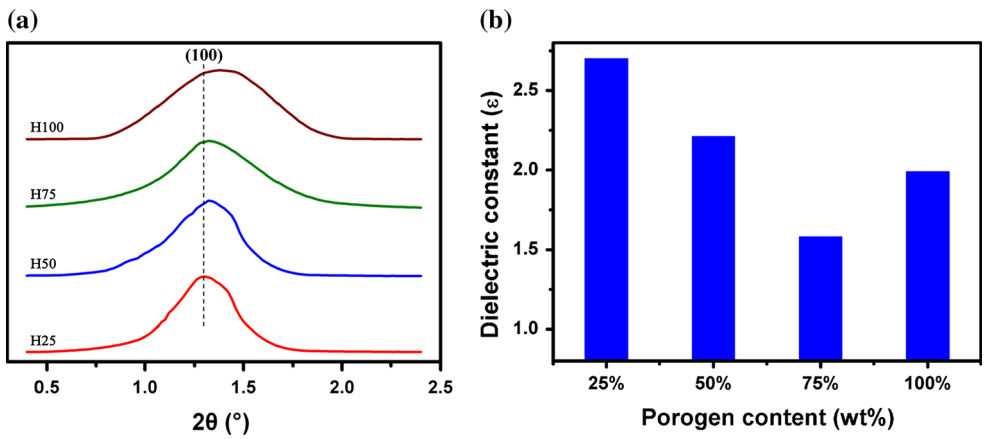

Figure 5 **a** XRD patterns and **b** dielectric properties of HFPDB-based PMO thin film with different weight ratios of porogen to precursor from 25 to 100 %.

with the presence of periodic mesoporous structure [33]. The peaks of the (100) reflection of HFPDB-based PMO films with different weight ratios of surfactant porogen to precursor are shifted to a higher angle, indicating the mesoporous structure contracts and the *d*-spacing decreases [14]. However, there are noticeable decrease in the XRD peak intensity and increase in the XRD peak width of samples

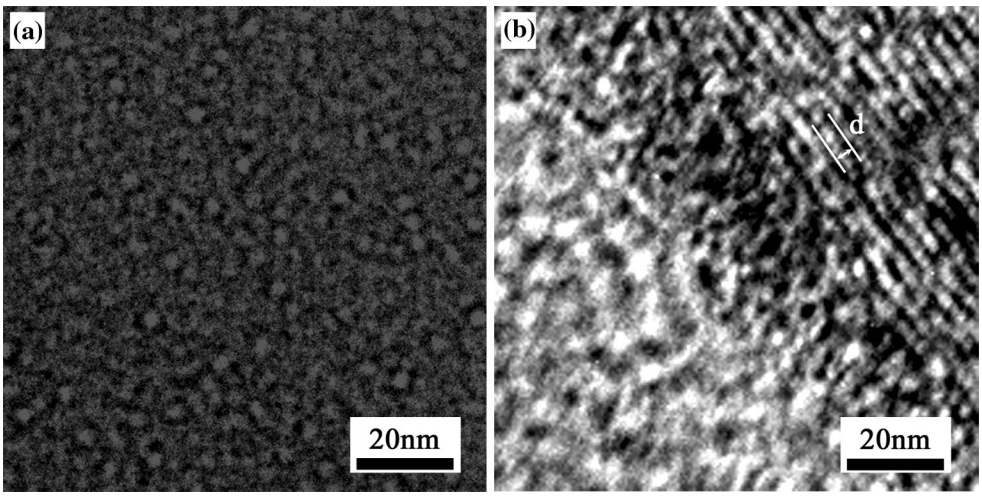

Figure 6 TEM images of H75 film sample **a** showing the wormhole structure and **b** showing the channel structure.

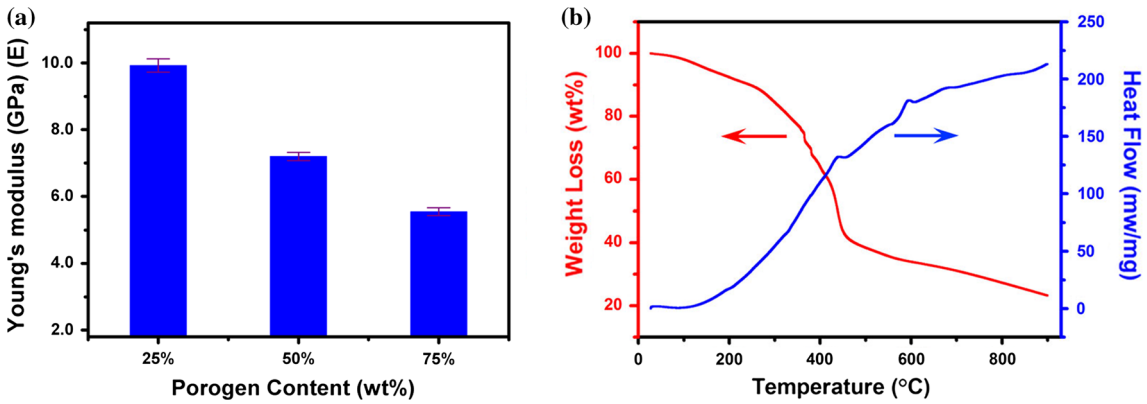

Figure 7 **a** Young's modulus of HFPDB-based PMO films with different porogen contents and **b** TGA-DSC curve for H75 PMO film.

from H25 to H100, which most likely originates from some disordering of the mesoporous structure by excess porogen. The order of mesoporous structure of H100 is the worst which is consistence with the result of SEM experiment. In pattern of H75, the strongest diffraction peak at 1.32° of 2θ, which associated with spacing (d) of 6.69 nm between the lattice planes.

Periodic mesoporous structure of as-prepared HFPDB-based PMO films has been proven through XRD characterization as above mentioned; their dielectric properties were further investigated by RF impedance analyzer. In order to reduce error, we used heavily doping silicon wafer (0.001–0.004 Ω) as substrate, and sputtered around 500 nm Cu layer on the as-prepared PMO thin films as electrode. According to result (Fig. 5b), the relative dielectric constant (κ) of samples reduced gradually with the increasing of porogen content at current frequency (1 MHz), and the κ value of H75 reduced to the lowest value of 1.58@1 MHz. However, the dielectric constant of H100 increased up to 1.99 compared with that of H75, which can be attributed to the disorder microstructure of H100 at high content of porogen. With the increase of porogen content, the leakage current of sample is trend to escalate. The leakage current density of H75 is 2.72×10^{-6} A cm^{-2} at applied voltage of 1 V and keeps it lower than 10^{-4} A cm^{-2} within 3 V, which was determined from I–V curves (Figure S2). Therefore, H75 sample with comparative order mesoporous structure and lowest dielectric constant can be considered as promising low-κ materials for next generation ILD.

To provide more evidence of the existence of such periodic mesoporous structure, the fragments

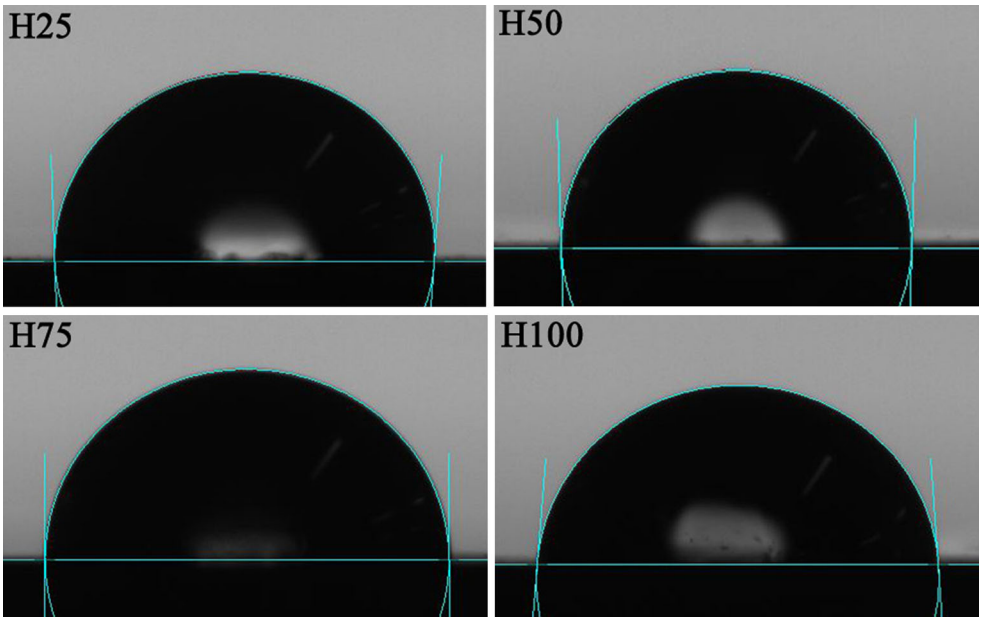

Figure 8 Water contact angle tests of HFPDB-based PMO thin film with different porogen contents.

scratched from the H75 sample were confirmed visually by TEM as shown in Fig. 6. In Fig. 6b, it can be seen that two kinds of microstructure including wormhole (bottom left) and channel (top right) structure were present in the HFPDB-based PMO thin film simultaneously. Thereinto, the wormhole structure represents regular mesopores (Fig. 6a) while channel structure represents the long-range two-dimensional hexagonal order (Fig. 6b). The microstructure of PMO is decided by porogen aggregates, influenced by its concentration, nature and around condition. The aggregated micelles always exist as worm-like shapes in low concentration solution but prefer to form channel-like entities when the porogen concentration exceeds its CMC. In same solution, different chemical conditions determine different microstructures. The micellar aggregates self-assemble to form channel-like entities, preferentially near the air-film and film-substrate interfaces, likely because of preferential wetting of air-film surface and film-substrate interfaces by a specific component [23]. Besides, the structure morphology is also coupled to the nature of precursor, which affects the hydrophilic-hydrophobic balance of porogen and degree of infusion [34]. TEM images also reveal the channel with a pore diameter of about 6 nm, which is consistent with the result of XRD characterization. Furthermore, the wormhole structure with slightly different sizes and mildly disordered arrangement can be ascribed of long carbon chain of bridged organic group in organosilane precursor, which imperils the long-range two-dimensional hexagonal order.

It is well known that higher porosity will result in lower κ-value as well as worse mechanical properties simultaneously. So it is necessary to investigate the mechanical properties for practical application by nanoindenter. Obviously, the Young's modulus of HFPDB-based PMO thin films declined with increasing weight ratio of porogen to precursor from 25 to 75 % as shown in Fig. 7a. Although bridged organic group and long carbon chain of precursor bring about disorder structure, it maintains high mechanical strength for the novel PMO thin film significantly. Additionally, the H75 PMO film with the lowest κ value possesses high Young's modulus of 5.54 $\pm$ 0.11 GPa, which satisfies the requirement of CMP [14]. Furthermore, the H100 thin film cannot acquire the Young's modulus value because its high porosity leads to fragile microstructure. Besides dielectric and mechanical properties, the thermogravimetric analysis (TGA) profile of the fragments of H75 was recorded under flowing nitrogen as shown in Fig. 7b. About 2 % mass loss attributed to residual water is observed between 27 and 100 °C. The mass decreases by 51.13 % from 100 to 442 °C, which is most likely due to a small loss of ethanol and water by the condensation of residual silanol and ethoxy groups in the EISA procedure. The TGA curve declines gently from 442 °C, which is most likely due

Table 2 Water contact angle and mechanical properties of HFPDB-based PMO films

Sample	Contact angle	E (GPa)
H25	93.1°	9.92 ± 0.20
H50	91.7°	7.20 ± 0.12
H75	90.1°	5.54 ± 0.11
H100	85.7°	<4.00

to the thermal decomposition of two kinds of acylamino group [35].

Finally, scientist pay much attention to the hydrophilicity of PMO film because that water has extremely polar O–H bonds and possesses much high dielectric constant close to 80 [2, 31]. The hydrophobicity of all HFPDB-based PMO films was characterized by contact angle meter as shown Fig. 8 and summarized in Table 2. It can be seen the contact angle decreased from 93.1° down to 90.1° with increasing of porogen content. However, the H75 PMO thin film also possess the hydrophobic property which is suitable for low-*k* applications.

Conclusions

In summary, we have developed a novel bridged organosilane (HFPDBO) precursor with star-shaped construction by a facile organic synthesis method. The as-prepared organosilane was used to prepare PMO thin film via EISA spin-coating procedure. The resultant HFPDB-based PMO film (H75) with 75 % of weight ratio of porogen to precursor possesses high mechanical property (Young's modulus of 5.54 ± 0.11 GPa) and excellent dielectric property (dielectric constants of 1.58@1 MHz) simultaneously. Finally, the H75 PMO thin film also shows superior thermal stability and hydrophobic property. In words, all the outstanding properties for low-*k* materials are present in the HFPDB-based PMO thin films which can be ascribed to the special molecular design. It can be considered as promising candidate for next generation low-*k* materials.

Acknowledgements

This work was financially supported by National Natural Science Foundation of China (Grant No. 21201175), Guangdong and Shenzhen Innovative Research Team Program (No. 2011D052, KYPT20121228160843692), and R&D Funds for basic Research Program of Shenzhen (Grant No. JCYJ20120615140007998, JCYJ20150401145529012).

Electronic supplementary material: The online version of this article (doi:10.1007/s10853-016-0066-6) contains supplementary material, which is available to authorized users.

References

[1] Martin SJ, Godschalx JP, Mills ME et al (2000) Development of a low-dielectric-constant polymer for the fabrication of integrated circuit interconnect. Adv Mater 12(12):1769–1778

[2] Shamiryan D, Abell T, Iacopi F et al (2004) Low-k dielectric materials. Mater Today 7(04):34–39

[3] Vora RH, Krishnan PSG, Goh SH et al (2001) Synthesis and properties of designed low-k fluoro-copolyetherimides. Part 1. Adv Funct Mater 11(5):361–373

[4] Morgen M, Ryan ET, Zhao JH et al (2000) Low dielectric constant materials for ULSI interconnects. Annu Rev Mater Sci 30(1):645–680

[5] Mcgahay V (2010) Porous dielectrics in microelectronic wiring applications. Materials 3(1):536–562

[6] Grill A, Neumayer DA (2003) Structure of low dielectric constant to extreme low dielectric constant SiCOH films: Fourier transform infrared spectroscopy characterization. J Appl Phys 94(10):6697–6707

[7] Kikuchi Y, Wada A, Kurotori T et al (2013) Non-porous ultra-low- k SiOCH (k = 2.3) for damage-free integration and Cu diffusion barrier. J Phys D-Appl Phys 46(39):395203–395209

[8] Xu J, Moxom et al (2002) Porosity in porous methylsilsesquioxane (MSQ) films. Appl Surf Sci 194(1):189–194

[9] Lee HJ, Soles CL, Liu DW et al (2004) Structural characterization of porous low-k thin films prepared by different techniques using x-ray porosimetry. J Appl Phys 95(5):2355–2359

[10] Geng Z, Huo M, Mu J et al (2014) Ultra low dielectric constant soluble polyhedral oligomeric silsesquioxane (POSS)–poly(aryl ether ketone) nanocomposites with excellent thermal and mechanical properties. J Mater Chem C 2(6):1094–1103

[11] Goethals F, Ciofi I, Madia O et al (2012) Ultra-low-k cyclic carbon-bridged PMO films with a high chemical resistance. J Mater Chem 22(17):8281–8286

[12] Maex K, Baklanov MR, Shamiryan D et al (2003) Low dielectric constant materials for microelectronics. J Appl Phys 93(11):8793–8841

[13] Hatton BD, Landskron K, Hunks WJ (2006) Materials chemistry for low-k materials. Mater Today 9(3):22–31

[14] Makoto S, Wendong W, Lofgreen JE et al (2011) Low-k periodic mesoporous organosilica with air walls: POSS-PMO. J Am Chem Soc 133(45):18082–18085

[15] Huang Y, Economy J (2006) New high strength low-k spin-on thin films for IC application. Macromolecules 39(39):1850–1853

[16] Lu HY, Teng CL, Kung CH et al (2011) Preparing mesoporous low-k films with high mechanical strength from noncrystalline silica particles. Ind Eng Chem Res 50(6):3265–3273

[17] Hunks WJ, Ozin GA (2005) Challenges and advances in the chemistry of periodic mesoporous organosilicas (PMOs). J Mater Chem 15:35–36

[18] Wills AW, Michalak DJ, Ercius P et al (2015) Block copolymer packing limits and interfacial reconfigurability in the assembly of periodic mesoporous organosilicas. Adv Funct Mater 25(26):4120–4128

[19] Hoffmann F, Cornelius M, Morell J (2006) Silica-based mesoporous organic-inorganic hybrid materials. Angew Chem Int Ed 45(20):3216–3251

[20] Barbara P, Andreas K, Thomas B (2011) Mesoporous structures confined in anodic alumina membranes. Adv Mater 23(21):2395–2412

[21] Edelstein D (2008) Extendibility of Cu/low-k/airgap BEOL. Electrochem Soc 28:2073

[22] Hatton B, Landskron K, Whitnall W et al (2005) Spin-coated periodic mesoporous organosilica thin films—towards a new generation of low-dielectric-constant materials. Adv Funct Mater 15(5):823–829

[23] Jiang T, Zhu B, Ding SJ et al (2014) High-performance ultralow dielectric constant carbon-bridged mesoporous organosilica films for advanced interconnects. J Mater Chem C 2(32):6502–6510

[24] Liu HC, Su WC, Liu YL (2011) Self-assembled benzoxazine-bridged polysilsesquioxanes exhibiting ultralow-dielectric constants and yellow-light photoluminescent emission. J Mater Chem 21(20):7182–7187

[25] Wang W, Lofgreen JE, Ozin GA (2010) Why PMO? Towards functionality and utility of periodic mesoporous organosilicas. Small 6(23):2634–2642

[26] Driessche IV, Der Voort PV (2013) Sealed ultra low-*k* organosilica films with improved electrical, mechanical and chemical properties. J Mater Chem C 1(25):3961–3966

[27] Yuan H, Xu J, Xie L (2011) Ultra low-dielectric-constant methylated mesoporous silica films with high hydrophobicity and stability. Mater Chem Phys 129(3):1195–1200

[28] Rathore JS, Interrante LV, Dubois G (2008) Adv Funct Mater 18(24):4022–4028

[29] Fiorilli S, Camarota B, Garrone E (2011) Carboxylic groups in mesoporous silica and ethane-bridged organosilica: effect of the surface on the reactivity. Phys Chem Chem Phys 13(3):1201–1209

[30] Wang W, Grozea D, Kohli S (2011) Water repellent periodic mesoporous organosilicas. ACS Nano 5(2):1267–1275

[31] Grosso D, Cagnol F, Soler-Illia GJAA (2004) Fundamentals of mesostructuring through evaporation-induced self-assembly. Adv Funct Mater 14(4):309–322

[32] Acharya A, Sanyal SK, Moulik SP (2001) Physicochemical investigations on microemulsification of eucalyptol and water in presence of polyoxyethylene (4) lauryl ether (Brij-30) and ethanol. Int J Pharm 229(1):213–226

[33] Landskron K, Hatton BD, Perovic DD (2003) Periodic mesoporous organosilicas containing interconnected $[Si(CH_2)]_3$ rings. Science 302(5643):266–269

[34] Pai RA, Watkins JJ (2006) Synthesis of mesoporous organosilicate films in supercritical carbon dioxide. Adv Mater 18(2):241–245

[35] Solymosi F, Bánsági T (1979) Infrared spectroscopic study of the adsorption of isocyanic acid. J Phys Chem 83(4):552–553